Journal of the Korean Ceramic Society
Vol. 55, No. 3, pp. 267~274, 2018.

https://doi.org/10.4191/kcers.2018.55.3.05

Synthesis and Characterization of TiO_2/CuS Nanocomposite Fibers as a Visible Light-Driven Photocatalyst

HyeLan An*, Leeseung Kang*, Hyo-Jin Ahn, Yong-Ho Choa***, and Chan Gi Lee*,†**

**Advanced Materials & Processing Center, Institute for Advanced Engineering, Yongin, 17180, Korea*
***Department of Materials Science and Engineering, Seoul National University of Science and Technology, Seoul 01811, Korea*
****Department of Fine Chemical Engineering, Hanyang University, Ansan 15588, Korea*

(Received February 2, 2018; Revised March 20, 2018; Accepted March 20, 2018)

ABSTRACT

TiO_2/CuS nanocomposites were fabricated by precipitation of nanosized CuS via sonochemical method on electrospun TiO_2 nanofibers, and their structure, chemical bonding states, optical properties, and photocatalytic activity were investigated. In the TiO_2/CuS nanocomposite, the position of the conduction band for CuS was at a more negative than that of TiO; meanwhile, the position of the valence band for CuS was more positive than those for TiO, indicating a heterojunction structure belonging to type-II band alignment. Photocatalytic activity, measured by decomposition of methylene blue under visible-light irradiation ($\lambda > 400$ nm) for the TiO_2/CuS nanocomposite, showed a value of 85.94% at 653 nm, which represented an improvement of 52% compared to that for single TiO_2 nanofiber (44.97% at 653 nm). Consequently, the photocatalyst with TiO_2/CuS nanocomposite had excellent photocatalytic activity for methylene blue under visible-light irradiation, which could be explained by the formation of a heterojunction structure and improvement of the surface reaction by increase in surface area.

Key words : Nanocomposite, Functional applications, Heterojunction, Electronic band structure, Photocatalytic activity

1. Introduction

The term photocatalyst, a combination of two words, "photo" and "catalyst," refers to a material or process that causes a catalytic reaction–an oxidation-reduction reaction–using light as an energy source. Photocatalysts have been drawing significant attention from various fields, such as air quality treatment and water treatment, due to their ability to decompose organic matter, odorous substances, bacteria, and viruses into water and carbon dioxide solely using light energy. Also, photocatalysts exhibit excellent bactericidal and antibacterial properties. A photocatalytic reaction is a process in which holes and electrons, formed by light irradiation in the valence and conduction bands, react with water, oxygen, OH^-, and H^+ on the surface of a photocatalytic material, generating OH radicals, which have strong oxidizing power. These OH radicals help decompose organic matter. TiO_2, ZnO, ZrO_2, and WO_3[1,2] are major photocatalytic materials, but many studies have been focusing on TiO_2, in particular, because it has optical activity but does not experience photocorrosion, thus exhibiting excellent durability, wear resistance, and oxidizing power. TiO_2, however, has a wide band gap of around 3.2 eV, and hence its photocatalytic characteristics are exhibited only in the ultraviolet spectral range (< 400 nm). As a result, when light with a wavelength ranging from 400 to 800 nm, i.e., the visible light spectrum range, is radiated, the delivered energy is not large enough to overcome the wide band gap of TiO_2, leading to the inability of the material to function as a photocatalyst. Accordingly, TiO_2 cannot absorb light in the visible spectral range, which accounts for 44% of sunlight, and reacts only with light in the ultraviolet range–only 5% of sunlight. This clearly shows the limitation of TiO_2 as a photocatalyst for sunlight-induced reactions. In attempts to overcome this limitation, many studies have been conducted on the development of a photocatalyst with a heterojunction structure capable of absorbing visible-light wavelengths and thus being activated. A heterojunction structure is designed by joining a material with a large band gap to a relatively small band-gap material to improve the absorptivity of visible-wavelength light. The structure also reduces hole-electron recombination and enhances the photocatalytic efficiency by promoting the migration and separation of electrons and holes generated by photoexcitation. Yeo *et al.* used a ball-mill process to synthesize a powder mix of TiO_2-WO_3 with a heterojunction structure by mixing TiO_2 nanoparticle–coated with Ag using a reduction-precipitation method–with WO_3 powder, which has a narrow band gap. As a result, the synthesized material exhibited improved photocatalytic activity under visible-wavelength light illumination. The improvement is ascribed to more effective separation of electrons and holes, where photo-excited electrons in WO_3 migrate towards TiO_2, instead of being recombined with holes.[3] Kim *et al.* formed a heterojunction

†Corresponding author : Chan Gi Lee
E-mail : cglee@iae.re.kr
Tel : +82-31-330-7495 Fax : +82-31-330-7116

structure by bringing together $FeTiO_3$ and TiO_2 nanoparticles synthesized via hydrothermal method. The holes, generated in $FeTiO_3$ by radiation of visual light, migrated into the valence band of TiO_2, enhancing the photocatalytic efficiency and activity in the visible spectral range.[4)]

CuS remains one of the most actively studied photocatalytic materials in the field due to its low price, non-toxicity, and narrow bandgap (up to 2.2 eV).[5)] The narrow bandgap of CuS allows the material to function as a photocatalyst in the visible spectral range. The present study aims to develop a photocatalyst capable of being activated in the visible spectral range by combining CuS and TiO_2, and thus forming a heterojunction structure. Also, the study intends to improve the photocatalytic activity by increasing the specific area for reaction via the addition of supported nanoparticles. To clarify the reasons for the photocatalytic property improvement, UV-vis analysis, XPS, and photocatalytic activity characterization were performed. This study is expected to provide a basis for future research on the effects of the band structure of heterogeneous semiconductor composites on photocatalytic properties.

2. Experimental Procedure

TiO_2/CuS nanocomposite fibers were produced using an electrospinning method and sonochemical method. 10 wt% of polyvinylpyrrolidone (PVP, $(C_6H_9NO)n$, Mw = 1,300,000 g/mol, Sigma-Aldrich), a type of polymer, and 10 wt% of titanium(IV) isopropoxide ($Ti[OCH(CH_3)_2]_4$, 97%, Sigma-Aldrich), a Ti Precursor, were added to N,N-Dimethylformamide (DMF, $HCON(CH_3)_2$, 99%, Sigma-Aldrich). After 1 h of dissolution, acetic acid (CH_3CO_2H, 99.7%, Sigma-Aldrich), a dispersing agent, was added to the solution. The prepared solution was transferred to a 20-ml syringe equipped with a 23-gauge stainless steel needle tip, and the solution in the syringe was set to flow at a rate of 0.05 ml/h by using a syringe pump. The distance between the needle tip and an Al collecting plate was set at about 10 cm, and a voltage of 9 to 11 kV was applied using a power supply. As-spun TiO_2 nanofibers, collected by electrospinning, were heat treated for 5 h at 500°C under atmosphere for removal of polymers and crystallization; and TiO_2 nanofibers were finally prepared. Also, TiO_2/Cu-seed nanofibers containing Cu seeds were produced by following the same process, except that 1 wt% of copper acetate ($Cu(CO_2CH_3)_2$, 98%, Sigma-Aldrich) was added to the solution. In preparation for forming TiO_2/CuS nanocomposite fibers, the synthesized TiO_2 and TiO_2/Cu-seed nanofibers were subject to agitation and ultrasonic waves in deionized water (DI water), so that all materials were uniformly dispersed. Subsequently, copper acetate, a Cu precursor, Thioacetamide (TAA, C_2H_5NS, 98%, Sigma-Aldrich), an S precursor, and Triethanolamine (TEA, $(OHCH_2CH_2)_3N$, 99%, Sigma-Aldrich), a complexing agent, were added at a weight ratio of 2 : 1 : 5 to the dispersed solution, leading to the formation of CuS nanoparticles, i.e., the existing TiO_2 nanofibers were composed with the newly formed CuS nanoparticles. The prepared materials were cleaned with distilled water and dried at 80°C; finally, TiO_2/CuS nanocomposite fibers were prepared. Also, an additional sample that was solely composed of CuS nanoparticles was prepared by following the above procedures. Therefore, the characteristics of CuS nanoparticles could be compared with those of TiO_2 nanofibers and TiO_2/CuS nanocomposite fibers.

Field-emission scanning electron microscopy (FESEM, Nova Nano SEM 450) was employed to analyze the shape and morphology of the prepared nanofibers. Transmission electron microscopy (TEM, JEM-2100F), along with an energy dispersive spectrometer (EDS) in mapping and line-scan mode, was used for crystal structure and compositional analysis. X-ray diffraction (XRD, Rigaku) was employed to study the composition and crystal structure of each phase: the scan was conducted in a range from 10 to 80 degrees at a rate of 2°/min. The UV/VIS spectrophotometer (JASCO V-730) was used to analyze the absorbance and bandgap, and X-ray photoelectron spectroscopy (XPS, Thermo Electron ESCALAB250 with Al Kα X-ray source) was applied to analyze the chemical bonding states. Based on the combined results of absorbance-based optical measurement of bandgaps and XPS measurement of the energy level of the valence band, the measured energy levels were schematized. Photocatalytic properties of samples were evaluated by the decomposition of methylene blue (MB) dye. Each sample was soaked at a concentration of 0.5 g/L in an MB aqueous solution with a concentration of 5×10^{-6} M. Subsequently, visible light exposure proceeded using a Xenon lamp (300 W) system equipped with a longpass filter (cut-on wavelength: 400 nm). Prior to the light exposure, the mixture of photocatalyst and dye solution was subject to 20 min of agitation in the dark to reach adsorption-desorption equilibrium. Subsequently, the solution was subject to 180 min of visible light exposure. During the light exposure, the solution was sampled at a constant time interval, and was analyzed to measure the absorbance of the remaining MB dye in the solution after the photodegradation process. The photodegradation rate was determined by calculating the ratio of the decrease in the absorbance rate after photodegradation to the initial absorbance rate of the MB dye measured at a wavelength of 653 nm.

3. Results and Discussion

Figure 1 shows XRD pattern analysis and FESEM images of TiO_2 nanofibers fabricated by electrospinning and CuS nanoparticles produced by sonochemical method. With regard to the nanofibers, the main diffraction peaks are observed at 25.3° and 37.89°, which correspond to the (101) and (004) planes of anatase TiO_2 (JCPDS card No. 84-1286), respectively, as well as at 27.5° and 36.1°, which correspond to the (110) and (101) planes of rutile TiO_2 (JCPDS card No. 87-0920), respectively. These observations imply that the nanofibers fabricated by electrospinning are TiO_2 composed

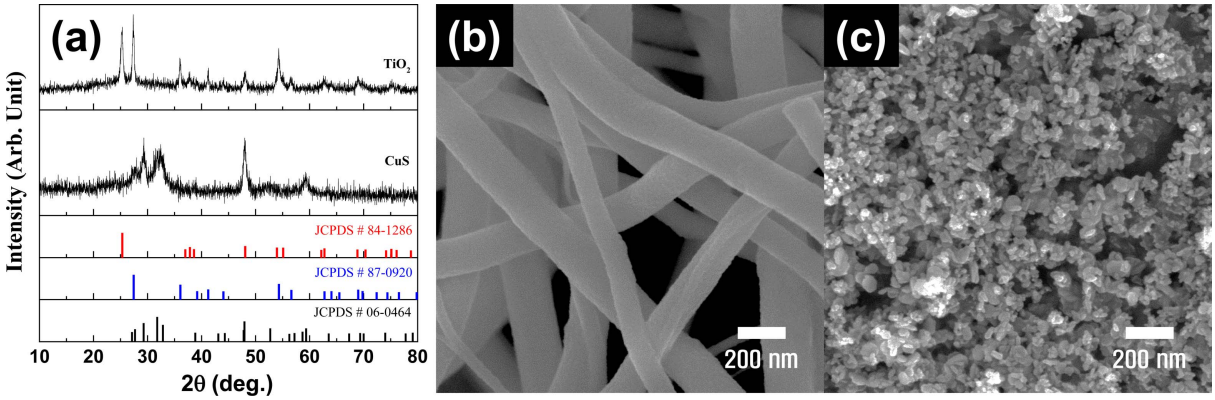

Fig. 1. (a) XRD data obtained from TiO_2 nanofiber and CuS nanoparticle. FESEM images of (b) TiO_2 nanofiber and (c) CuS nanoparticle.

of anatase and rutile TiO_2. For the nanoparticles, the main diffraction peaks are observed at 29.2°, 31.7°, and 47.9°, which correspond to the (102), (103), and (110) planes of CuS (JCPDS card No. 06-0464), demonstrating that the nanoparticles fabricated by the sonochemical method are hexagonal-shaped CuS nanoparticles. As shown in the FESEM images in Fig. 1(b-c), TiO_2 is a type of nanofiber with a diameter of 110 to 145 nm, and has a smooth surface. CuS is a sphere-shaped particle with a size of 30 to 70 nm. The results of the XRD and FESEM analyses confirm that TiO_2 nanofibers and CuS nanoparticles were successfully fabricated by the electrospinning method and sonochemical method, respectively.

Subsequently, the sonochemical method was employed to form the CuS nanoparticles with the TiO_2 nanofibers; the results are shown in Fig. 2. When CuS was formed on the nanofiber solely composed of TiO_2, the nanofibers could not remain intact in shape, i.e., broken-shaped nanofibers observed, as shown in Fig. 2(a). This phenomenon may be due to the following reasons. First, during the calcination process following the electrospinning of the TiO_2 nanofibers, PVP polymers in the nanofibers were eliminated, leading to a decrease in relative density of the nanofibers, and thus possibly causing contraction and internal stress. Accordingly, the TiO_2 nanofibers become unstable and vulnerable to breakage.[6,7] Second, these unstable TiO_2 nanofibers were subsequently subject to ultrasonic treatment and other

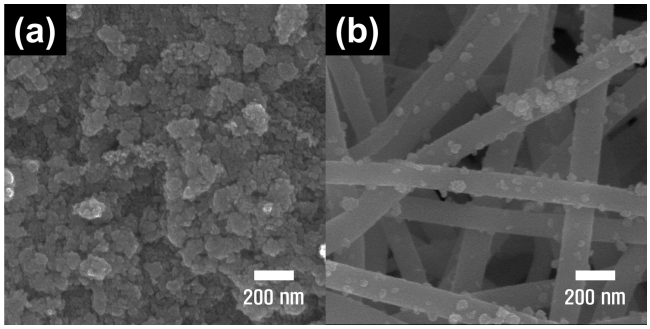

Fig. 2. FESEM images of TiO_2/CuS nanocomposite synthesized using TiO_2 nanofiber (a) without Cu-seed, and (b) with Cu-seed.

chemical processes for the synthesis of CuS, which probably caused physical and chemical damage. In attempts to supplement the mechanical strength degradation of the TiO_2 nanofibers after the calcination process, and relieve the stress applied to the nanofibers during the synthesis process of CuS, Cu nano-seeds were introduced into the nanofibers. As a result, TiO_2/CuS nanocomposite fibers were fabricated, and it was observed that these fibers remained intact in shape, as shown in Fig. 2(b). SEM and TEM analyses were performed to analyze the characteristics of the Cu-seeds introduced into the TiO_2 nanofibers and also to investigate in depth the effect of the Cu-seeds on composite for-

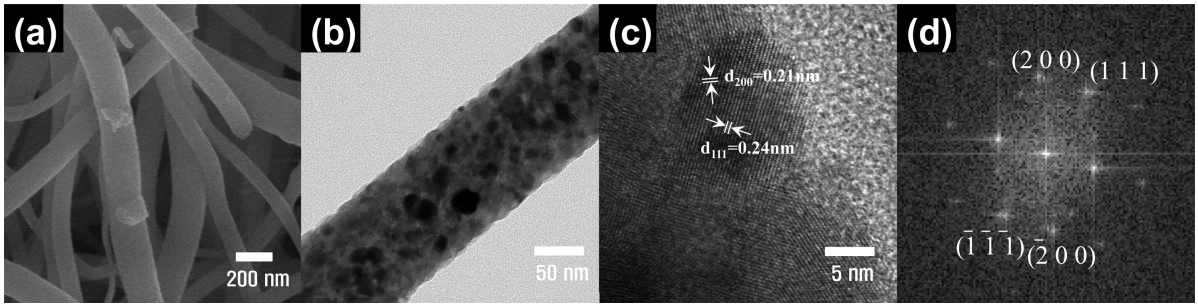

Fig. 3. (a) FESEM image of TiO_2/Cu-seed nanofiber. (b) TEM image of TiO_2/Cu-seed nanofiber. (c) High-resolution TEM image of TiO_2/Cu-seed nanofiber; corresponding characteristic FFT is shown in (d).

mation.

Figure 3 shows the results of the SEM and TEM analyses, which were performed to analyze the morphology and crystal structure of the TiO_2/Cu-seed nanocomposite fibers fabricated using the electrospinning method. A TiO_2/Cu-seed nanocomposite fiber fabricated by electrospinning is shaped as a one-dimensional nanofiber with a diameter of 122 to 185 nm. Its surface shows no significant difference compared to that of a typical TiO_2 nanofiber. As a result of Fast Fourier Transformation (FFT) diffraction pattern analysis, however, the crystalline phase of Cu_2O (JCPDS card No. 75-1531) was observed in localized regions, and this observation implied that the Cu acetate added to form nanofibers was oxidized to form the Cu_2O phase. The observed Cu_2O phase has a lattice constant of 4.27 Å, and hence it can relive the lattice mismatch between TiO_2 (4.5937 Å) and CuS (3.792 Å). This helps strengthen the adhesion between TiO_2 and CuS when a TiO_2/CuS nanocomposite fiber is formed, and reduces the risk of misfit dislocation. It is thought that these factors helped the TiO_2 nanofibers remain intact in shape. Therefore, Cu_2O contained in nanofibers is considered to help improve the strength of TiO_2/Cu_2O nanofibers by suppressing the Zener pinning effect and reliving the misfit between rutile TiO_2 and CuS. It also serves as a seed for the formation of CuS[8] when CuS nanoparticles are formed on the surface of TiO_2 by using the

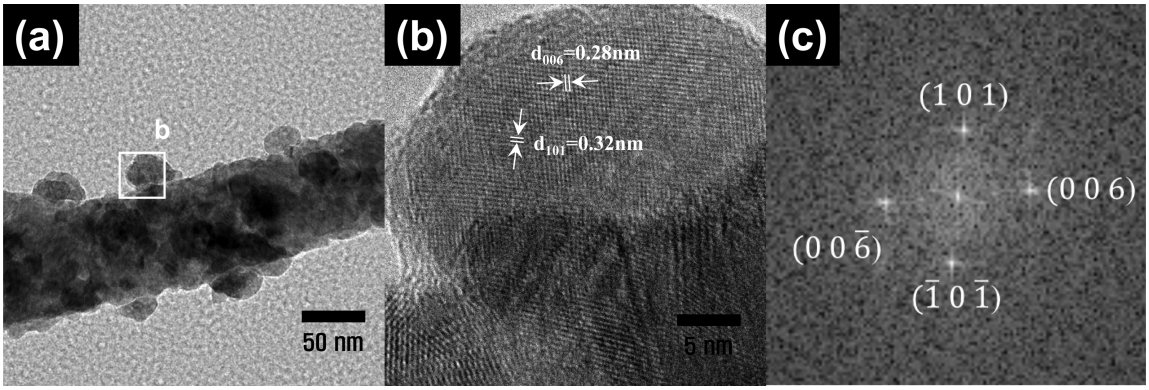

Fig. 4. (a) TEM image of TiO_2/CuS composite. (b) High-resolution TEM image of TiO_2/CuS composite; the corresponding characteristic FFT is shown in (c).

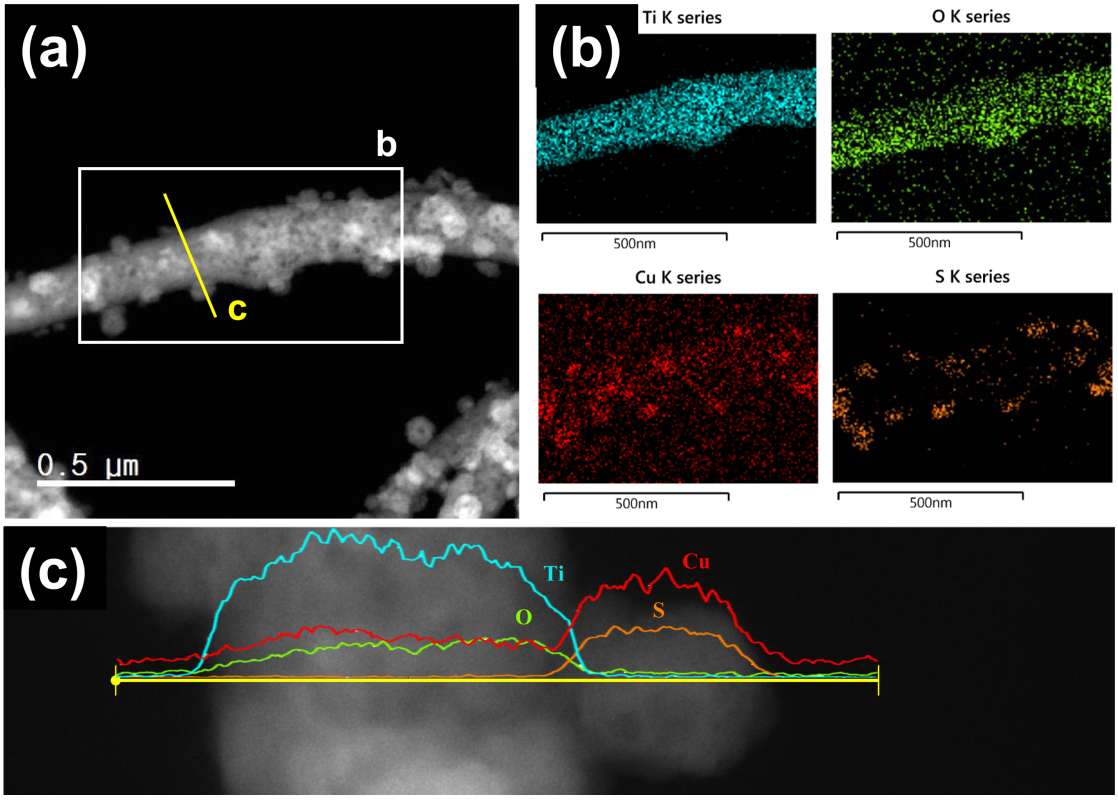

Fig. 5. (a) Bright-field TEM image of TiO_2/CuS composite, (b) EDS mapping and (c) line scan for Ti, O, Cu, and S elements of TiO_2/CuS composite.

sonochemical method. In sum, it is thought that Cu_2O contributes to the formation of TiO_2/Cu_2O nanocomposite fibers.

CuS nanoparticles, formed on the surface of TiO_2/CuO_2-seed nanofibers by using the sonochemical method, were sphere-shaped nanoparticles with a size of 34 to 67 nm. The shape and size of these CuS nanoparticles, as shown in Fig. 4(a), were similar to those of the solely synthesized CuS nanoparticles, as shown in Fig. 1(c). HRTEM analysis was performed to more closely observe the sphere-shaped nanoparticles formed on the surface of the nanofibers. The results are shown in Fig. 4(b) and the corresponding FFT diffraction pattern is shown in Fig. 4(c). As a result of the FFT diffraction pattern analysis, it was found that the observed planes corresponded to the (101) and (006) planes of hexagonal-shaped CuS (JCPDS card No. 06-0464). This confirms that CuS nanoparticles were successfully synthesized on the surface of TiO_2/CuO_2-seed nanofibers. EDS mapping and line scan analysis were conducted to investigate the phase formation and element distribution of the synthesized nanofiber composites. As shown in Fig. 5(a) and (b), the EDS mapping analysis was conducted on a nanofiber and a sphere-shaped nanoparticle formed on the nanofiber surface for elements including Ti, O, Cu, and S. The results show that the distribution of Ti and O corresponds with that of the nanofiber. The distribution of S, which composes CuS, tends to correspond with the that of the nanoparticle region formed on the nanofiber surface, but Cu is distributed not only across the nanoparticle, along with S, but also, to some extent, across the nanofiber region on which the nanoparticle sits. However, considering that Cu is less densely distributed across the nanofiber region compared to Ti or O, the corresponding Cu counts are thought to come from Cu-seeds, which were added for the formation of TiO_2 nanofibers. This implies that elemental Cu was uniformly distributed to form Cu-seeds when TiO_2 nanofibers were formed. Also, elemental Cu successfully formed CuS nanoparticles on the surface of the nanofibers. These findings are confirmed by the results of the EDS line-scan analysis, as shown in Fig. 5(c). It is observed that elemental Ti and O are found in the nanofiber region without being diffused into the nanoparticle region, while S is found in the nanoparticle region without being diffused into the nanofiber region. As mentioned above, elemental Cu was present not only in the CuS nanoparticle region but also in the nanofibers, along with Ti and O; this indicates the uniform formation of Cu-seeds across these nanofibers. Therefore, it can be concluded that TiO_2/CuS nanocomposite fibers were successfully fabricated without any interfacial diffusion or chemical composition change during the formation of the TiO_2/Cu-seed nanofibers, produced by electrospinning, together with CuS nanoparticles produced by the sonochemical method. The sonochemical method-based composition process of CuS nanoparticles was reported to follow the mechanism below.[9]

$$H_2O \Rightarrow H\cdot + OH\cdot \text{ (by ultrasound)} \quad (1)$$

$$H\cdot + CH_3CSNH_2 \Rightarrow H_2S + CH_3(NH_2)C\cdot \quad (2)$$

$$Cu^{2+} + xTEA \Leftrightarrow [Cu(TEA)_x]^{2+}\cdot \quad (3)$$

$$Cu^{2+} + H_2S \Rightarrow CuS + 2H^+ \quad (4)$$

The formation of CuS can be summarized using the above equations: Eq. (1) describes the formation of a hydrogen radical (H ·) from the ultrasonic dissociation of water; Eq. (2) describes the formation of H_2S from the reaction between a hydrogen radical (H ·) and TAA; Eq. (3) describes the formation of Cu-TEA composites and emission of a Cu^{2+} ion from the Cu^{2+}-TEA complexation; and Eq. (4) describes the synthesis process of CuS from the reaction between Cu^{2+} and H_2S. These CuS nanoparticles formed on the surface of the TiO_2 nanofibers tend to have a large specific surface area,[10] thus contributing to enhanced photodegradation properties, because photodegradation is a type of surface reaction.[10,11]

With regard to semiconductor materials, the absorption wavelengths of the material are closely linked to its bandgap. Therefore, the absorbance of TiO_2 nanofibers and CuS nanoparticles was analyzed to identify the range of wavelengths at which absorption takes place, as shown in Fig. 6(a). XPS analysis was conducted by normalizing the measured valence band spectra and, as a result, the energy level of the valence band was determined with the Fermi level used as a reference, as shown in Fig. 6(b). Each bandgap of each sample was calculated by substituting into the equation $E = hc/\lambda$ the wavelength measured from the extrapolation of the ultraviolet-visible spectrum of the sample. The

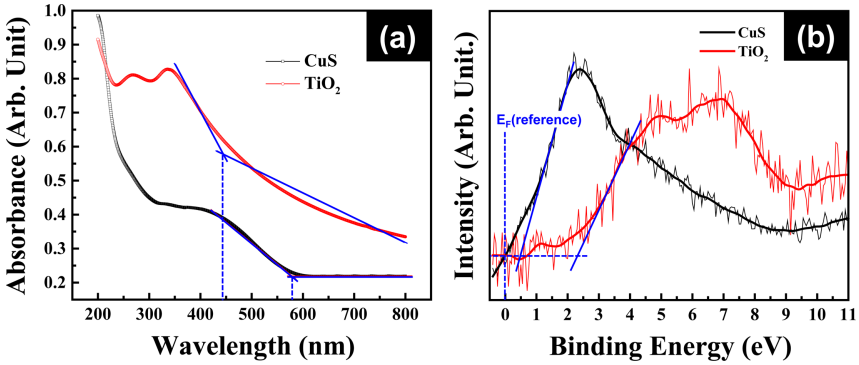

Fig. 6. (a) UV-vis absorption spectra, (b) Normalized XPS valence band spectra of CuS and TiO_2.

Table 1. Band Gap and Calculated Conduction Band (CB) and Valence Band (VB) Positions of CuS and TiO_2

Sample	Band gap (eV)	CB (eV)	VB (eV)
CuS	2.1	- 1.6	0.5
TiO_2	2.8	- 0.4	2.4

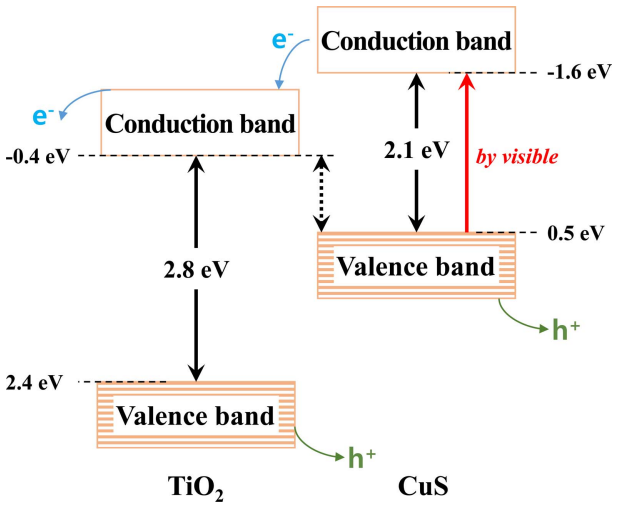

Fig. 7. Scheme for energy band structures of CuS and TiO_2.

valence band maximum (VBM) was determined by using the background line to extrapolate the edge of the spectrum. Results are shown in Table 1.

Based on the absorbance measurements in Fig. 6 and the chemical-bonding data in Table 1, the energy level-diagram for the TiO_2/CuS nanocomposite fibers was achieved, as shown in Fig. 7. Also, the migration of the electrons and holes generated when CuS nanoparticles are excited by visible light is schematized in the same figure. Likewise, in a heterojunction where two different semiconductors are joined, the corresponding energy band alignment is determined by the relative position of the energy levels of the two semiconductors. In general, heterojunctions are divided into three types.[12] Absorbance and chemical-bonding analysis (Fig. 5) shows that the energy levels of the valence band and conduction band of TiO_2 are lower than those of CuS, which demonstrates that the TiO_2/CuS nanocomposite fibers in the present study correspond to Type-II heterojunction structures (staggered gap). CuS nanoparticles have a narrow band gap of 2.1 eV, and hence electrons and holes could be generated and separated under visible light illumination. Part of these electrons in the conduction band of CuS quickly migrate into TiO_2 because the energy level of the conduction band of CuS is higher than that of TiO_2. The electrons and holes transferring from CuS to TiO_2 generate hydroxyl radicals (OH), strong oxidizers, triggering a photocatalytic reaction,[13] and this type of energy band alignment, as a result, makes it possible for the TiO_2/CuS nanocomposite fibers to be activated in the visible light spectrum range. To analyze the activation reaction and photocatalytic prop-

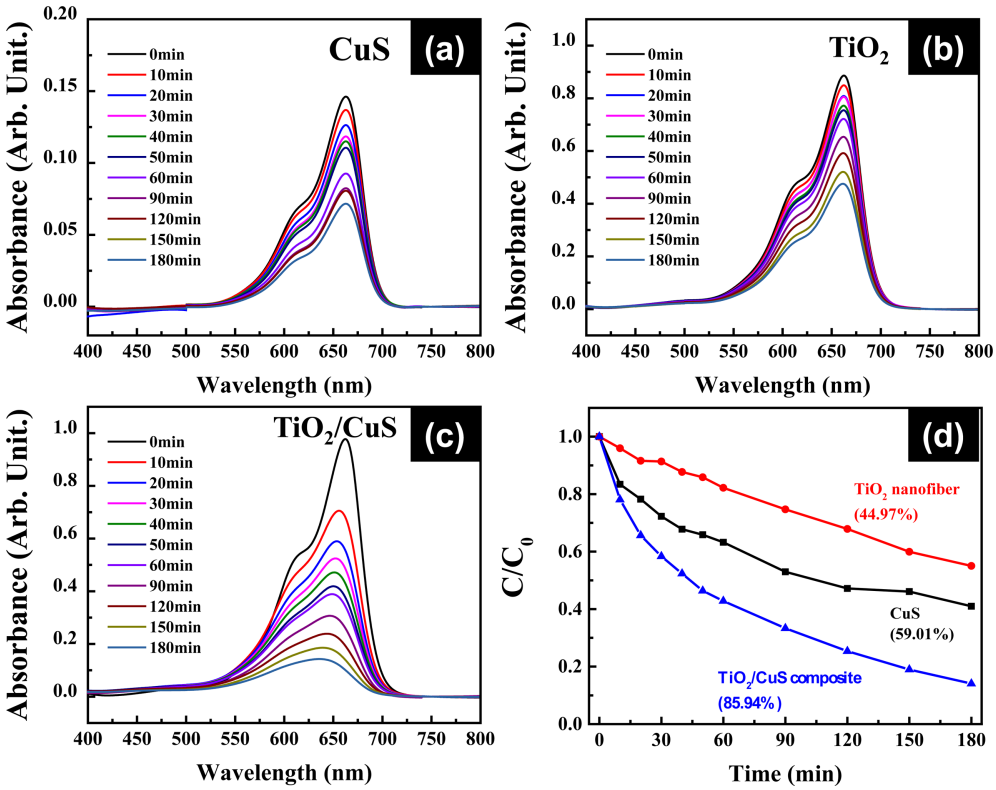

Fig. 8. UV-vis absorption spectra of methylene blue solution at different time intervals in presence of (a) CuS, (b) TiO_2 nanofiber, and (c) TiO_2/CuS composite; (d) photodegradation rate of methylene blue under visible radiation with CuS, TiO_2 nanofiber, and TiO_2/CuS composite.

erties under visible light illumination, the synthesized TiO_2/CuS nanocomposite fibers were analyzed with respect to the photodegradation of MB dye, and the result was compared with those of CuS nanoparticles and TiO_2 nanofibers, as shown in Fig. 8.

For more efficient assessment of photocatalytic activity in the visible light spectrum range, the Xenon lamp system equipped with longpass filter ($\lambda > 400$ nm) was used. It was found that the absorbance of the target solution gradually decreased with the visible light irradiation time because MB dye in the solution is gradually decomposed by the photocatalytic effect. Based on the absorbance, the photodegradation rate, which reflects the photocatalytic effect of the sample, can be determined by using the equation below.[14] The results are plotted as shown in Fig. 8(d).

$$D\ (\%) = (C_0 - C_i) / C_0 \times 100$$

Here, D refers to the photodegradation rate, C_0 is the initial concentration of MB dye, and C_i is the MB dye concentration after i h of treatment. TiO_2 generally exhibits excellent photodegradation activity, and thus is widely used as a typical photocatalyst material; however, its large bandgap makes it unable to absorb light in the visible spectral range. For that reason, despite 180 min of visible light exposure, the photodegradation efficiency of the TiO_2 nanofibers (~ 2.8 eV) was found to be approximately 44.97%, which results from its low photodegradation activity. In the case of CuS nanoparticles (~ 2.1 eV), which have a narrower bandgap, the photodegradation efficiency was up to 59.01%, and the efficiency of the TiO_2/CuS nanocomposite fibers that had been formed was even higher at 85.94%. The improved photocatalytic efficiency can be attributed to the following two factors. First, the TiO_2/CuS nanocomposite fibers, due to their nanoparticle formation, have a specific surface area larger than that of the TiO_2 nanofibers. Second, the formation with CuS, which has a relatively narrow bandgap (2.1 eV), led to the formation of a Type II heterojunction structure, which allows the absorption of light not only in the ultraviolet spectral region but also in the visible spectral region. In sum, the increased specific surface area and extension of absorption wavelength range contributed to improving the photocatalytic property of the TiO_2/CuS nanocomposite fibers: the photodegradation efficiency was 85.94%, which was 52% larger than that of the TiO_2 nanofibers, i.e., 44.97%.

4. Conclusions

In the present study, TiO_2 nanofibers with diameters in a range of 110 to 145 nm were fabricated using the electrospinning method. To formation of TiO_2/CuS nanocomposite nanofibers, Cu_2O-seeds, which help improve stability and also act as seeds for the formation of CuS nanoparticles, were introduced into the TiO_2 nanofibers. Subsequently, the composition process proceeded using the sonochemical method, in which CuS nanoparticles with sizes of 34 to 67 nm were uniformly formed in the nanofibers. As a result, TiO_2/CuS nanocomposite fibers were successfully fabricated by combining TiO_2/Cu-seed nanofibers produced by electrospinning with CuS nanoparticles obtained using the sonochemical method. XRD, HR-TEM, and EDS analyses show that the TiO_2/CuS nanocomposite fibers contain nanofibers composed of anatase and rutile TiO_2 and Cu_2O-seeds; the CuS nanoparticles are adsorbed on the surface of the nanofibers. The synthesized TiO_2/CuS nanocomposite fibers were analyzed with respect to the photodegradation of MB dye. The photodegradation efficiency of the nanocomposite fibers was found to be 85.94%, which was 52% larger than that of the TiO_2 nanofibers (44.97%). The improved photocatalytic efficiency is attributed to the enhanced surface reaction activity caused by the increased specific surface area of the nanocomposite fibers, resulting from their being formed with nanoparticles. Also, the Type II heterojunction structure of the nanocomposite fibers, which contained CuS nanoparticles with a narrow bandgap, made it possible for this material to absorb light in the visible spectral region. Considering that the synthesized TiO_2/CuS nanocomposite fibers exhibit excellent photocatalytic activity even under visible light illumination, the technology developed in the present study has significant potential for use in the photodegradation of organic pollutants.

Acknowledgments

This work was supported by Industrial Critical Technology Development Program (10062526, Development of Chalcogenide-based Ceramic Composites for Energy-efficient Windows (visible light transmission, > 70%, infrared cutoff, > 90%)), funded by the Ministry of Trade, Industry & Energy, Republic of Korea.

REFERENCES

1. A. Ali and W. C. Oh, "Photocatalytic Performance of CoS_2-Graphene-TiO_2 Ternary Composites for Reactive Black B (RBB) Degradation," *J. Korean Cream. Soc.*, **54** [4] 308-13 (2017).
2. S. Kang, R. C. Pawar, T. J. Park, J. G. Kim, S. H. Ahn, and C. S. Lee, "Minimization of Recombination Losses in 3D Nanostructured TiO_2 Coated with Few Layered g-C_3N_4 for Extended Photo-response," *J. Korean Cream. Soc.*, **53** [4] 393-99 (2016).
3. I. C. Yeo and I. C. Kang, "Preparation of WO_3-TiO_2 Photocatalyst and Evaluation of Its Photo-Activity in the Visible Light Range," *J. Kor. Powd. Met. Inst.*, **20** [6] 474-78 (2013).
4. Y. J. Kim, B. Gao, S. Y. Han, M. H. Jung, A. K. Chakraborty, T. Ko, C. Lee, and W. I. Lee, "Heterojunction of $FeTiO_3$ Nanodisc and TiO_2 Nanoparticle for a Novel Visible Light Photocatalyst," *J. Phys. Chem. C*, **113** [44] 19179-84 (2009).
5. M. Saranya, C. Santhosh, R. Ramachandran, P. Kollub, P. Saravanan, M. Vinoba, S. K. Jeong, and A. N. Grace,

"Hydrothermal Growth of CuS Nanostructures and Its Photocatalytic Properties," *Powder Technol.,* **252** 25-32 (2014).
6. N. Horzum, R. Muñoz-Espí, G. Glasser, M. M. Demir, K. Landfester, and D. Crespy, "Hierarchically Structured Metal Oxide/Silica Nanofibers by Colloid Electrospinning," *ACS Appl. Mater. Interfaces*, **4** [11] 6338-45 (2012).
7. A. E. Deniz, A. Celebioglu, F. Kayaci, and T. Uyar, "Electrospun Polymeric Nanofibrous Composites Containing TiO_2 Short Nanofibers," *Mater. Chem. Phys.*, **129** [3] 701-4 (2011).
8. M. A. Kanjwal, N. A. M. Barakat, F. A. Sheikh, S. J. Park, and H. Y. Kim, "Photocatalytic Activity of ZnO-TiO_2 Hierarchical Nanostructure Prepared by Combined Electrospinning and Hydrothermal Techniques," *Macromol. Res.*, **18** [3] 233-40 (2010).
9. H. Wang, J. R. Zhang, X. N. Zhao, S. Xu, and J. J. Zhu, "Preparation of Copper Monosulfide and Nickel Monosulfide Nanoparticles by Sonochemical Method," *Mater. Lett.*, **55** [4] 253-58 (2002).
10. G. Hu, X. Meng, X. Feng, Y. Ding, S. Zhang, and M. Yang, "Anatase TiO_2 Nanoparticles/Carbon Nanotubes Nanofibers: Preparation, Characterization and Photocatalytic Properties," *J. Mater. Sci.*, **42** [17] 7162-70 (2007).
11. S. M. Kim, T. K. Yun, and D. I. Hong, "Effect of Rutile Structure on TiO_2 Photocatalytic Activity," *J. Korean Chem. Soc.*, **49** [6] 567-74 (2005).
12. L. M. Lacroix, F. Delpech, C. Nayral, S. Lachaize, and B. Chaudret, "New Generation of Magnetic and Luminescent Nanoparticles for in Vivo Real-Time Imaging," *Interface Focus*, **3** [3] 20120103 (2013).
13. N. Qin, Y. Liu, W. Wu, L. Shen, X. Chen, Z. Li, and L. Wu, "One-Dimensional CdS/TiO_2 Nanofiber Composites as Efficient Visible-Light-Driven Photocatalysts for Selective Organic Transformation: Synthesis, Characterization, and Performance," *Langmuir*, **31** [3] 1203-9 (2015).
14. L. Zhu and W. C. Oh, "Novel Bi_2S_3/TiO_2 Heterogeneous Catalyst: Photocatalytic Mechanism for Decolorization of Texbrite Dye and Evaluation of Oxygen Species," *J. Korean Cream. Soc.*, **53** [1] 56-62 (2016).